

In Defense of the Triplet Loss for Visual Recognition

Ahmed Taha¹, Yi-Ting Chen², Teruhisa Misu², and Larry Davis¹

¹University of Maryland, College Park

²Honda Research Institute, USA

{ahmdtaha, lsd}@umiacs.umd.edu {ychen, tmisu}@honda-ri.com

Abstract

We employ triplet loss as a space embedding regularizer to boost classification performance. Standard architectures, like ResNet and DesneNet, are extended to support both losses with minimal hyper-parameter tuning. This promotes generality while fine-tuning pretrained networks. Triplet loss is a powerful surrogate for recently proposed embedding regularizers. Yet, it is avoided for large batch-size requirement and high computational cost. Through our experiments, we re-assess these assumptions.

During inference, our network supports both classification and embedding tasks without any computational overhead. Quantitative evaluation highlights how our approach compares favorably to the existing state of the art on multiple fine-grained recognition datasets. Further evaluation on an imbalanced video dataset achieves significant improvement (> 7%). Beyond boosting efficiency, triplet loss brings retrieval and interpretability to classification models.

1. Introduction

Standard architectures [8, 30] are powerful classification models. Pretrained ImageNet [5] weights scale their strength through fine tuning to novel domains and relax the large labeled dataset requirement. Unfortunately, these models suffer from overfitting. This reduces generality on unseen data especially for minority classes. To limit overfitting, we utilize triplet loss [26] as a classification regularizer, during training or fine-tuning, to boost accuracy. It promotes a better embedding space by attracting similar and repelling different classes. This embedding also raises classification model interpretability by enabling nearest neighbor retrieval.

Embedding losses have been successfully applied in conjunction with softmax loss as regularizers. Initially, center loss [35] was proposed for better face recognition efficiency.

Magnet loss [23] generalizes the unimodality assumption of center loss. A recent triplet-center loss (TCL) [9] uses only a unimodal embedding but introduced a repelling force between class centers, i.e. inter-class margin maximization. All these methods assume a fixed number of embedding modes by computing class representatives during training.

Unlike the aforementioned approaches, we neither compute class centers nor impose an explicit number of embedding modes. Triplet loss promotes compactness and margin maximization. To enable multi-modal embedding, a semi-hard sampling strategy is utilized. While previous methods employ custom architectures, we extend standard networks to integrate our regularizer. This integration achieves state-of-the-art results through promoting better embedding. Figure 1 shows our two head architecture where the pre-logit convolutional layer supports both classification and embedding heads. Pre-logits are projected into an embedding space using triplet loss while supporting the softmax loss.

We evaluate our approach on various classification domains. The first is a fine-grained visual recognition (FGVR). The second domain is an ego-motion action recognition task with high class imbalance. Comparable state-of-the-art results are achieved on the former and significant improvement on the latter domain. Evaluation on multiple architectures with the same hyper-parameters highlights our approach's generality. The large batch size requirement represents a key challenge for triplet loss adoption. In our experiments, we show that using a small batch size $b = 33$ still leads to good results. A further qualitative evaluation shows our regularizer adds values in terms of interpretability.

In summary, the key contributions of this paper are:

1. Integration of triplet loss, incorporating semi-hard negative sampling, in standard architectures,
2. Increased classification model interpretability,
3. A reassessment of the large batch size requirement to utilize triplet loss,
4. State-of-the-art results on various fine-grained visual

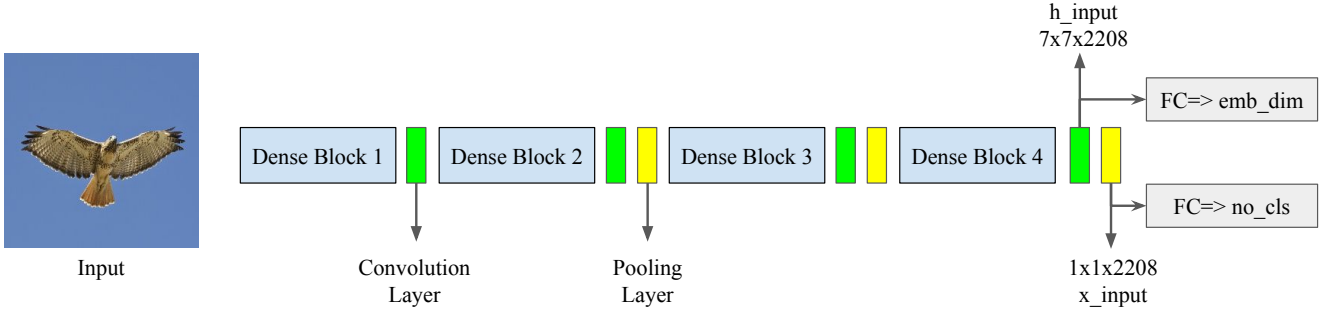


Figure 1: Our proposed two-head architecture builds on standard networks – DenseNet used for visualization, $x_{input} = pool(h_{input})$. Besides computing classification logits, the pre-logits layer supports object embedding. Softmax and triplet losses are applied to the classification logits and embedding respectively.

recognition datasets with minimal hyper parameter tuning.

2. Related Work

Visual recognition deep networks employ softmax loss as follows

$$L_{soft} = - \sum_{i=1}^b \log \frac{e^{W_{y_i}^T x_i + b s_{y_i}}}{\sum_{j=1}^n e^{W_{y_j}^T x_i + b s_{y_j}}} \quad (1)$$

where $x_i \in R^d$ denotes the i th deep feature, belonging to the y_i th class. In standard architectures, x_i is the pre-logit layer; the result of flattening the pooled convolutional features as shown in figure 1. $W_j \in R^d$ denotes the j th column of the weights $W \in R^{d \times n}$ in the last fully connected layer and $bs \in R^n$ is the bias term. b and n are the batch size and the number of class respectively. The softmax loss forces samples from different classes apart. Yet, class compactness and inter-class margin maximization are disregarded due to neural networks overfitting capabilities. Embedding regularization is one way to tackle this limitation.

2.1. Center Loss

Wen *et al.* [35] propose center loss to minimize intra-class variations. By maintaining a per class representative feature vector $c_{y_i} \in R^d$, the novel loss term in equation 2 is proposed. The class centers are computed by averaging corresponding class features. They are updated after every training mini-batch. To avoid perturbations caused by noisy samples, a hyper-parameter α controls the learning rate of the centers, i.e. moving average.

$$L_{cen} = \frac{1}{2} \sum_{i=1}^b \|x_i - c_{y_i}\|_2^2 \quad (2)$$

2.2. Magnet Loss

Rippel *et al.* [23] propose a center loss term supporting multi-modal embedding– magnet loss. It computes K class representatives, i.e. K -clusters per class. Each sample is iteratively assigned to one of the K clusters and pushed towards its center. The magnet loss adaptively sculpts the representation space by identifying and enforcing intra-class variation and inter-class similarity. This is formulated as follows

$$L_M = \frac{1}{N} \sum_{i=1}^N - \log \frac{e^{\frac{-1}{2\sigma^2} \|x_i^k - \mu_k^c\|_2^2} - \alpha}{\sum_{c \neq C(x_i^k)} \sum_{k=1}^K e^{\frac{-1}{2\sigma^2} \|x_i^k - \mu_k^c\|_2^2} - \alpha} \quad (3)$$

where N and K are the number of samples and clusters per class respectively. $x_i^k \in R^d$ denotes the i th deep feature, belonging to cluster k in the y_i th class, $\mu_k^c \in R^d$ is the k th cluster center belonging to class c . Finally $\sigma^2 = \frac{1}{N-1} \sum \|x_i^k - \mu_k^c\|_2^2$ is the variance of all samples from their respective centers. One criticism of magnet loss is the complexity overhead to maintain multiple clusters per class and their assigned samples. Imbalanced data distributions also conflict with the requirement of having a constant number of clusters per class.

2.3. Triplet Center Loss

While promoting class compactness, the center loss depends on the softmax loss supervision signal to push different classes apart. The learned features optimized with the softmax loss supervision signal are not discriminative enough, i.e. no explicit repelling force pushes different classes apart. Inter-class clusters can overlap due to missing an explicit inter-class repelling incentive. He *et al.* [9] propose triplet center loss (TCL) to avoid this limitation. By maintaining a per class center $c_{y_i} \in R^d$ similar to [35],

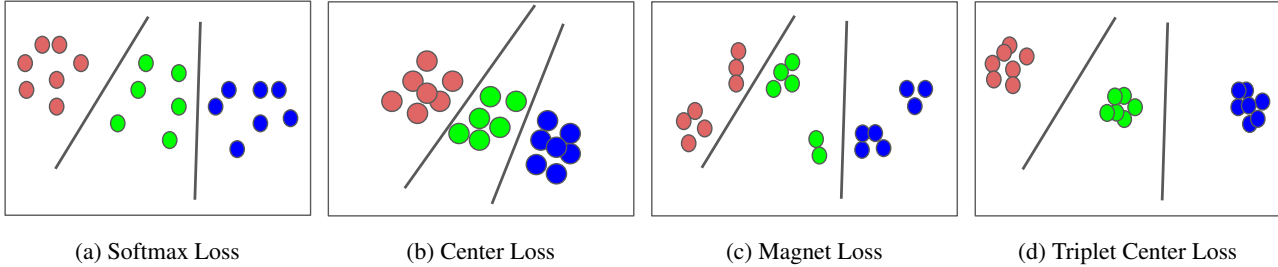


Figure 2: Visualization of different losses objectives. Softmax separates samples with neither class compactness nor margin maximization considerations. Center loss promotes unimodal compact class while magnet loss supports multi-modal embedding. Triplet center loss strives for unimodal, margin maximization and class compactness.

TCL is formulated as follows

$$L_{tcl} = \sum_{i=1}^b \left[(D(x_i, c_{y_i}) - \min_{j \neq i} D(x_i, c_{y_j}) + m) \right]_+ \quad (4)$$

where m is a separating margin, $[\cdot]_+ = \max(0, \cdot)$ and $D(\cdot)$ represents the squared Euclidean distance function.

Triplet loss is a well-established surrogate for TCL. It achieves the intra and inter class embedding objectives without computing class centers. Yet, it is largely avoided for its computational complexity and large training batch requirement claims. In the experiment section, we address these concerns and evaluate the ability of triplet loss to boost performance. Our approach is evaluated on the challenging FGVR task where intra-class overwhelm inter-class variations. Further evaluation on the Honda driving dataset (HDD) demonstrates our approach’s competence on an imbalanced video dataset.

3. The Triplet Loss Regularizer

The next subsection introduces triplet loss [26] as a softmax loss regularizer. Then, we explain our standard architectural extension to integrate an embedding loss.

3.1. Triplet Loss

Triplet loss [26] has been successfully applied in face recognition [26, 25] and person re-identification [3, 29, 24]. In both domains, it is used as a space embedding tool to measure similarity between objects and provide a metric for clustering. In this work, we utilize triplet loss as a classification regularizer. It is more efficient than contrastive loss [7, 16], and less computationally expensive than quadruplet [12, 2] and quintuplet [11] losses. While the pre-logits layer learns better representations for classification using the softmax loss, triplet loss promotes a better space embedding. Equation 5 shows the triplet loss formulation

$$L_{tri} = \frac{1}{b} \sum_{i=1}^b [(D(a, p) - D(a, n) + m)]_+ \quad (5)$$

where an anchor image a of a specific class is pushed closer to all other positive images p from the same class than it is to any negative image n of any other class. Equation 6 is our loss function with a balancing hyper-parameter λ .

$$L = L_{soft} + \lambda L_{tri} \quad (6)$$

Triplet loss performance is dependent on its sampling strategy. We follow the semi-hard sampling strategy proposed in [26]. In semi-hard negative sampling, instead of picking the hardest positive-negative samples, all anchor-positive pairs and their corresponding semi-hard negatives are considered. Semi-hard negatives satisfy equation 7. They are further away from the anchor than the positive exemplar, yet within the banned margin m . Figure 3 shows a triplet loss tuple and highlights different types of negative exemplars.

$$D(a, p) < D(a, n) < D(a, p) + m \quad (7)$$

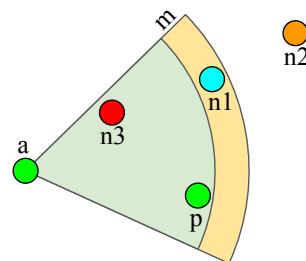


Figure 3: Triplet loss tuple (anchor, positive, negative) and margin m . Hard, semi-hard and easy negatives highlighted in red, cyan and orange respectively.

An easy negative satisfies the margin constraint and suffers a zero loss. Unlike hard-sampling, semi-hard sampling supports a multi-modal embedding. Hard sampling

picks the farthest positive and nearest negative without any consideration for the margin. In contrast, semi-hard sampling ignores hard negatives. Figures 4 illustrates this. Two classes, red and green, are embedded into one and two clusters respectively. A hard sampling strategy pulls the farthest positive from one cluster to the anchor in the other cluster, i.e. promotes a merge. The semi-hard sampling strategy omits this tuple because the negative sample is nearer than the positive.

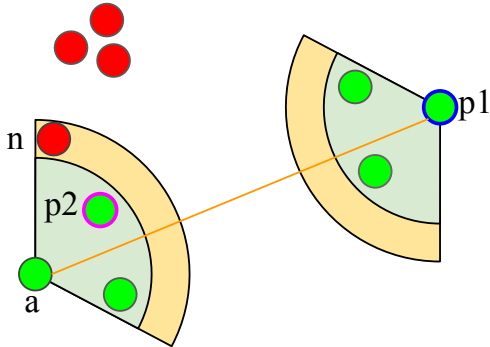


Figure 4: Hard sampling promotes unimodal embedding by picking the farthest positive and nearest negative $(a, p1, n)$. Semi-hard sampling picks $(a, p2, n)$ and avoids any tuple (a, p, n) where n lies between a and p .

The existence of a semi-hard negative is not guaranteed in small batches, especially near convergence. Thus, we prioritize negative exemplars as illustrated in figure 3. First priority is given to semi-hard, then easy and finally hard negatives.

3.2. Network Architecture

Standard architectures are employed in various applications for their powerful imageNet [5] weights. Pre-trained networks relax the large labeled dataset requirement, save training time and achieve better performance. Losses, like center and triplet-center loss, lose this advantage by employing custom architectures. We seek to leverage pre-trained standard networks for their advantages in tasks like fine-grained recognition [18, 15, 14].

Unlike VGG [28], recent architectures [8, 31, 13] end with a convolutional layer before the final logit layer. To generate logits, the convolutional layer is pooled, flattened, then multiplied by a customizable fully connected layer to support various numbers of classes. We propose a similar extension to integrate triplet loss. Before pooling, we flatten the convolutional layer then apply another fully connected layer W_{emb} to generate embeddings as illustrated in equa-

	Flowers-102 [21]	Aircrafts [20]	NABirds [33]
Num Classes	102	100	550
Avg samples Per Class	10	100	43.5
Train Size	1020	3334	23929
Val Size	1020	3333	N/A
Test Size	6149	3333	24633

Table 1: FGVR datasets summary

tion 9.

$$logits = W_{logits} * flat(x) \tag{8}$$

$$embedding = W_{emb} * flat(h) \tag{9}$$

where $x = pool(h)$. Orderless pooling, like averaging, ignores feature locations. Thus, a fully connected layer W_{emb} applied on h has finer control level. Different embedding dimensionality is feasible by tuning W_{emb} dimensions. The final embedding is normalized to the unit-circle and the square Euclidean distance metric is employed. During inference, our proposed two-head architecture enables both classification and retrieval without additional overhead.

4. Experiments

4.1. Evaluation on FGVR

We evaluate our approach on three FGVR datasets. These datasets comprise both make/model classification and wildlife species. The **Aircrafts** dataset contains 10,000 images of aircraft spanning 100 aircraft-models. The finer level differences between models makes visual recognition challenging. The **NABirds** dataset contains 48,562 images across 550 visual categories of North American birds. Finally, the **Flower-102** dataset contains 8189 images across 102 classes. These datasets provide challenges in terms of large intra-class but small inter-class variations. Table 1 summarizes the datasets' size, number of classes and splits. Figure 5 presents samples from the three datasets.

All experiments are conducted on Titan Xp 12GB GPU. By default, the hyper-parameter $\lambda = 1$, triplet loss margin $m = 0.2$, embedding dimensionality $d_{emb} = 256$. All networks are initialized with ImageNet weights, and fine-tuned for 20K iterations. We use batch-size $b = 33$ for a fair comparison with triplet loss approach. Momentum optimizer is utilized with momentum 0.9 and a polynomially decaying learning rate $lr = 0.1$. To evaluate our approach, batches



Figure 5: Sample evaluation images. The first, second and third rows show samples from NABirds, Flower-102 and Aircrafts dataset respectively.

are constructed to contain both positive and negative samples.

We follow the batch construction procedure proposed in Hermans *et al.* [10]. A class is uniformly sampled then $K = 4$ sample images, with resolution 224×224 , are randomly drawn. Training images are augmented online with random crops and horizontal flipping. This process iterates until a batch is complete. Table 2 shows our quantitative evaluation based on fine-tuning a pre-trained DenseNet on the three datasets. Both the baseline and our approach are evaluated five times. Average top 1 accuracy and standard deviation are reported. Supplementary material provides the detailed experiment results.

4.2. Architectures Generalization

To illustrate the competence of our approach on standard architectures, it is evaluated on ResNet-50. While DenseNet achieves better performance, it comes with a higher computational cost for its internal aggregation links. Inception [31] and ResNet [8] are lighter residual networks compared to DenseNet. One key observation is the similarity between all these networks' last trainable layers. A typical pattern is a convolutional layer, pooling, then a fully connected layer to generate N -classes predictions.

Table 3 displays the results using Resnet-50 with the same hyper-parameters used for DenseNet. The superior results, achieved on the three datasets, highlight the generality of our approach.

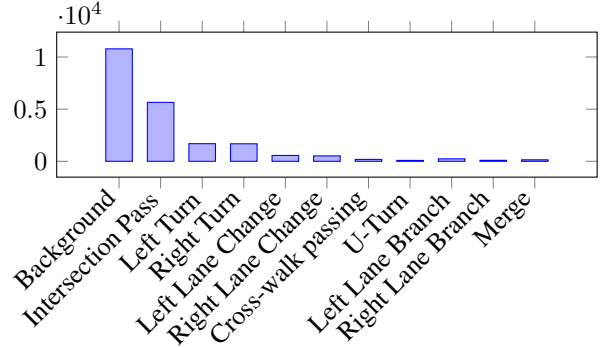


Figure 6: Honda driving dataset long tail class distribution

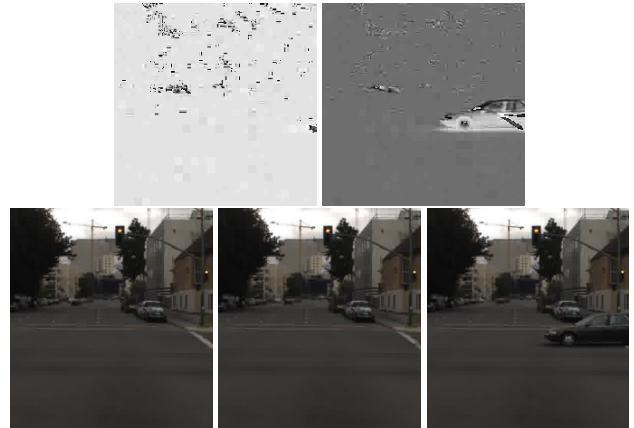


Figure 7: Stack of difference motion encoding. Instead of six frames, three are used for visualization purpose. The first row shows a stack of two difference frames constructed by subtracting consecutive pairs of grayscale frames in the second row. These images are best viewed in color/screen.

4.3. Task Generalization

We next evaluate on the Honda driving dataset (HDD) [22] for action recognition. HDD is an ego-motion video dataset for driver behavior understanding and causal reasoning. It contains 10833 events spanning eleven event classes. The HDD event class distribution is long-tailed which poses an imbalance data challenge. Figure 6 shows the eleven event classes with their distributions. To reduce video frames redundancy, they are sampled at 3 Hz (three frames per second), and events shorter than 2 seconds are omitted.

To leverage standard architecture for action recognition, Fernando *et al.* [6] stack of difference (SOD) motion encoding is adopted. While better motion encoding like optical-flow exists, the SOD is utilized for its simplicity and ability to achieve competitive results [6, 32]. Given a sequence of frames representing an event, six consecutive frames spanning 2 seconds are randomly sampled. They are converted

Flowers-102		Aircrafts		NABirds	
Method	Acc	Method	Acc	Method	Acc
Det.+Seg. [1]	80.66	Wang et al. [34]	85.70	Branson et al. [36]	35.70
Overfeat [27]	86.80	Liu et al. [19]	86.80	Van et al. [15]	75.00
Softmax	93.09±0.37	Lin et al. [17]	92.00	Softmax	78.77±0.08
Soft+Tri (Ours)	94.34±0.35	Cui et al. [4]	92.40	Soft+Tri (Ours)	79.71±0.07
		Softmax	88.53±0.38		
		Soft+Tri (Ours)	89.47±0.28		

Table 2: Quantitative evaluation on the three FGVR datasets. Softmax indicates baseline performance using DenseNet161

Flowers-102		NABirds	
Method	Acc	Method	Acc
Softmax	84.85	Softmax	65.91
Soft+Tri (Ours)	84.97	Soft+Tri (Ours)	66.33

Aircrafts	
Method	Acc
Softmax	83.13
Soft+Tri (Ours)	85.87

Table 3: Quantitative evaluation to illustrate architecture generalization. Softmax indicates baseline performance using ResNet-50

to grayscale, and then every consecutive pair is subtracted to create a stack of difference $\in \mathbb{Z}^{W \times H \times 5}$ as depicted in figure 7. Standard architectures are easily adapted to this input representation by treating the SOD input as a five-channel image instead of three.

Unlike FGVR input $\in [0, 255]$, $SOD \in [-255, 255]$. Thus, a ResNet50 [8] architecture initialized with random weights is employed. It is trained for 10K iterations with a hyper-parameter $\lambda = 1$ and a polynomially decaying learning rate $lr = 0.01$. Batch sizes 33 and 63 are used to compare the vanilla softmax against our approach. To highlight performance on minority classes, both micro and macro average accuracies are reported in table 4. Macro-average computes the metric for each class independently before taking the average. Micro-average is the traditional mean for all samples. Macro-average treats all classes equally while micro-averaging favors majority classes. Table 5 highlights the efficiency of our approach on minority classes.

4.4. Hyper-Parameter Stability

Our approach has two hyper-parameters: λ and the embedding dimensionality d_{emb} . λ is tuned on the Flowers-102 dataset through the validation split. All hyper-parameter tuning experiments are executed for 2000 iterations. Figure 8 highlights λ stability within $[0.1, 2]$. Softmax loss rapidly converges to zero, especially on pre-trained architectures. Through our experiments, we found

	Micro Acc	Macro Acc
Softmax ($b = 33$)	84.43	47.66
Softmax+Triplet ($b = 33$)	84.93	53.70
Softmax ($b = 63$)	84.45	46.53
Softmax+Triplet ($b = 63$)	84.85	54.08

Table 4: Action recognition quantitative evaluation on the Honda dataset. b indicates the batch-size used. Macro average accuracy highlights performance on minority classes.

Event	Soft	Ours	Soft	Ours
	Batch-size 33		Batch-size 63	
Background	96.28	95.29	97.32	96.28
Intersection Passing	74.61	75.86	74.26	74.68
Left Turn	85.49	84.87	85.18	86.11
Right Turn	88.47	87.22	86.91	86.60
Left Lane Change	59.40	66.33	55.44	62.37
Right Lane Change	44.79	61.45	40.62	51.04
Cross-walk Passing	18.18	18.18	12.12	12.12
U-Turn	0.00	11.76	0.00	23.52
Left Lane Branch	53.84	64.10	41.02	64.10
Right Lane Branch	0.00	6.24	12.49	18.74
Merge	3.22	19.35	6.45	19.35
Macro Accuracy	47.66	53.70	46.53	54.08

Table 5: Detailed evaluation on the Honda driving dataset. Softmax plus triplet loss achieves better performance on minority classes.

that triplet loss intervention is better delayed until softmax convergence. Thus, a larger λ making triplet loss dominant is discouraged. d_{emb} is dependent on dataset size; we use $d_{emb} = 256$ to accommodate various datasets size.

Further λ and d_{emb} tuning per-dataset achieves better performance but brings extra cost in terms of hyper-parameters tuning. We give up these improvements to highlight the generality of our approach.

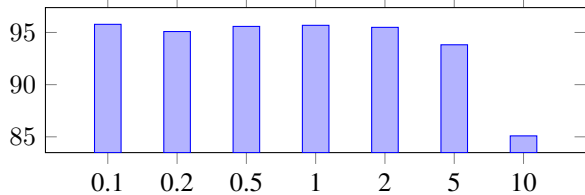


Figure 8: Hyper-parameter λ tuning on the Flowers-102 dataset.

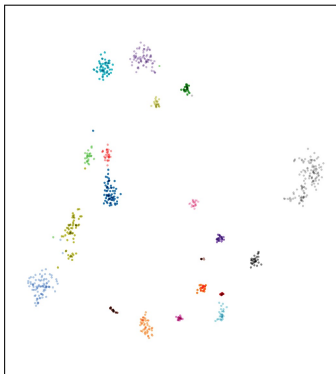


Figure 9: t-SNE visualization for Flowers-102 embedding space using 20 random classes, 40 samples per class. Best viewed in color.

4.5. Retrieval Evaluation

Semi-hard negative sampling and the extra computational cost to learn W_{emb} increase the training duration. We justify this overhead by supporting retrieval and raising the classification model interpretability. Retrieval performance is presented in table 6. The reported classification accuracy provides an upper bound for retrieval. In our experiments, test and train splits act as the query and gallery database respectively. Retrieval and classification top 1 accuracies are comparable. The retrieval top 5 accuracy is superior to the classification top 1 on two datasets. Figure 9 shows a t-SNE visualization for Flowers-102 embedding space using 20 random classes, 40 samples per class. Due to t-SNE visualization inconsistency, even with fixed parameters, more runs are visualized in the supplementary material.

Figure 10 presents our qualitative evaluation. The query image, in the first column, is followed by its nearest four neighbors. The figure illustrates the value added to the classification model by our proposed architecture. Nearest neighbors can serve as an explanation of a classification decision. This enables noise and outlier detection in labeled datasets. An incorrect classification due to scarce annotations become easier to explain. The second, fourth and sixth rows reveal corner cases. A human intervention can address these by manually correcting noisy or adding tailored an-

	Flowers-102	Aircrafts	NABirds
Classification Top 1	94.34	89.47	79.71
Retrieval Top 1	91.06	88.93	76.29
Retrieval Top 5	94.29	90.94	84.25
Retrieval mAp	90.68	88.41	70.16

Table 6: Retrieval quantitative evaluation against classification as an upper bound. Both retrieval and classification top 1 are comparable. Retrieval top 5 is superior to classification top 1 on both Aircrafts and NABirds datasets.

notations. A finer level of annotation understanding helps raise labeled datasets quality. This would raise classification model accuracy.

4.6. Discussion

Our experiments demonstrate how triplet loss can boost softmax loss performance. Triplet loss attains the center loss, triplet center loss and magnet loss objectives without enforcing explicit class representatives. It promotes both class compactness and margin maximization. Semi-negative sampling relaxes the unimodal embedding constraint. Through triplet loss integration in pre-trained standard architecture, comparable state-of-the-art results were obtained on fine grained recognition tasks. Our approach is three times slower due to the CPU semi-hard sampling procedure. An optimized GPU implementation will reduce training duration.

To promote generality, we fix our hyper-parameter $\lambda = 1$ in all experiments. Tuning λ to achieve further improvements is an application dependent trade-off. Thus, we only demonstrate stability within a reasonable range. Triplet loss effectively regularizes softmax and reduces over-fitting.

5. Conclusion

We propose a seamless integration of triplet loss into standard classification architectures. Our triplet loss regularizer competence is illustrated using different datasets, architectures and recognition tasks. Triplet loss, without the large batch requirement, boosts softmax performance. With minimal hyper-parameter tuning and using pretrained standard architectures, we promote generality to novel domains. Promising results are achieved on an imbalanced dataset. We incur a computational overhead during training, but raise classification model interpretability. Our architectural extension enables both retrieval and classification tasks during inference.

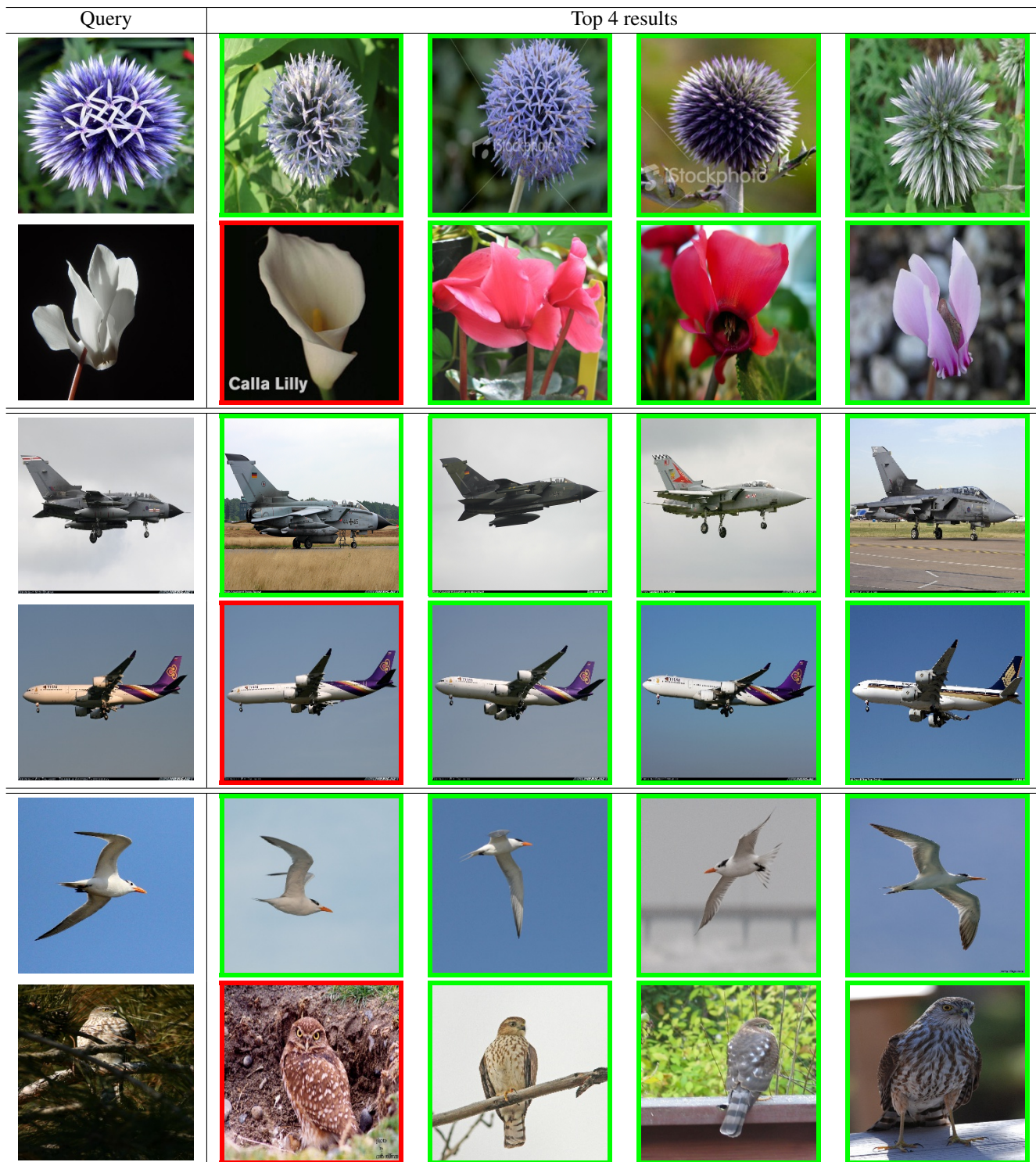


Figure 10: Qualitative evaluation on the three FGVR datasets. Beside the query image, in the first column, the top four results are presented. Correct and incorrect results are highlighted in green and red respectively. Nearest neighbors help explain a misclassification and raise the classification model interpretability.

References

- [1] A. Angelova and S. Zhu. Efficient object detection and segmentation for fine-grained recognition. In *Proceedings of the*

- tion, pages 811–818, 2013. 6
- [2] W. Chen, X. Chen, J. Zhang, and K. Huang. Beyond triplet loss: a deep quadruplet network for person re-identification. In *The IEEE Conference on Computer Vision and Pattern Recognition (CVPR)*, volume 2, 2017. 3
- [3] D. Cheng, Y. Gong, S. Zhou, J. Wang, and N. Zheng. Person re-identification by multi-channel parts-based cnn with improved triplet loss function. In *Proceedings of the IEEE Conference on Computer Vision and Pattern Recognition*, pages 1335–1344, 2016. 3
- [4] Y. Cui, F. Zhou, J. Wang, X. Liu, Y. Lin, and S. J. Belongie. Kernel pooling for convolutional neural networks. In *CVPR*, volume 1, page 7, 2017. 6
- [5] J. Deng, W. Dong, R. Socher, L.-J. Li, K. Li, and L. Fei-Fei. Imagenet: A large-scale hierarchical image database. In *Computer Vision and Pattern Recognition, 2009. CVPR 2009. IEEE Conference on*, pages 248–255. Ieee, 2009. 1, 4
- [6] B. Fernando, H. Bilen, E. Gavves, and S. Gould. Self-supervised video representation learning with odd-one-out networks. In *CVPR*, 2017. 5
- [7] R. Hadsell, S. Chopra, and Y. LeCun. Dimensionality reduction by learning an invariant mapping. In *null*, pages 1735–1742. IEEE, 2006. 3
- [8] K. He, X. Zhang, S. Ren, and J. Sun. Deep residual learning for image recognition. In *Proceedings of the IEEE conference on computer vision and pattern recognition*, pages 770–778, 2016. 1, 4, 5, 6
- [9] X. He, Y. Zhou, Z. Zhou, S. Bai, and X. Bai. Triplet-center loss for multi-view 3d object retrieval. *arXiv preprint arXiv:1803.06189*, 2018. 1, 2
- [10] A. Hermans, L. Beyer, and B. Leibe. In defense of the triplet loss for person re-identification. *arXiv preprint arXiv:1703.07737*, 2017. 5
- [11] C. Huang, Y. Li, C. Change Loy, and X. Tang. Learning deep representation for imbalanced classification. In *Proceedings of the IEEE Conference on Computer Vision and Pattern Recognition*, pages 5375–5384, 2016. 3
- [12] C. Huang, C. C. Loy, and X. Tang. Local similarity-aware deep feature embedding. In *Advances in Neural Information Processing Systems*, pages 1262–1270, 2016. 3
- [13] G. Huang, Z. Liu, L. Van Der Maaten, and K. Q. Weinberger. Densely connected convolutional networks. In *CVPR*, volume 1, page 3, 2017. 4
- [14] J. Krause, H. Jin, J. Yang, and L. Fei-Fei. Fine-grained recognition without part annotations. In *Proceedings of the IEEE Conference on Computer Vision and Pattern Recognition*, pages 5546–5555, 2015. 4
- [15] J. Krause, B. Sapp, A. Howard, H. Zhou, A. Toshev, T. Duerig, J. Philbin, and L. Fei-Fei. The unreasonable effectiveness of noisy data for fine-grained recognition. In *European Conference on Computer Vision*, pages 301–320. Springer, 2016. 4, 6
- [16] Y. Li, Y. Song, and J. Luo. Improving pairwise ranking for multi-label image classification. In *The IEEE Conference on Computer Vision and Pattern Recognition (CVPR)*, 2017. 3
- [17] T.-Y. Lin and S. Maji. Improved bilinear pooling with cnns. *arXiv preprint arXiv:1707.06772*, 2017. 6
- [18] T.-Y. Lin, A. RoyChowdhury, and S. Maji. Bilinear cnn models for fine-grained visual recognition. In *Proceedings of the IEEE International Conference on Computer Vision*, pages 1449–1457, 2015. 4
- [19] M. Liu, C. Yu, H. Ling, and J. Lei. Hierarchical joint cnn-based models for fine-grained cars recognition. In *International Conference on Cloud Computing and Security*, pages 337–347. Springer, 2016. 6
- [20] S. Maji, E. Rahtu, J. Kannala, M. Blaschko, and A. Vedaldi. Fine-grained visual classification of aircraft. *arXiv preprint arXiv:1306.5151*, 2013. 4
- [21] M.-E. Nilsback and A. Zisserman. Automated flower classification over a large number of classes. In *Computer Vision, Graphics & Image Processing, 2008. ICVGIP'08. Sixth Indian Conference on*, pages 722–729. IEEE, 2008. 4
- [22] V. Ramanishka, Y.-T. Chen, T. Misu, and K. Saenko. Toward driving scene understanding: A dataset for learning driver behavior and causal reasoning. In *CVPR*, 2018. 5
- [23] O. Rippel, M. Paluri, P. Dollar, and L. Bourdev. Metric learning with adaptive density discrimination. *arXiv preprint arXiv:1511.05939*, 2015. 1, 2
- [24] E. Ristani and C. Tomasi. Features for multi-target multi-camera tracking and re-identification. *arXiv preprint arXiv:1803.10859*, 2018. 3
- [25] S. Sankaranarayanan, A. Alavi, C. Castillo, and R. Chelappa. Triplet probabilistic embedding for face verification and clustering. *arXiv preprint arXiv:1604.05417*, 2016. 3
- [26] F. Schroff, D. Kalenichenko, and J. Philbin. Facenet: A unified embedding for face recognition and clustering. In *Proceedings of the IEEE conference on computer vision and pattern recognition*, pages 815–823, 2015. 1, 3
- [27] A. Sharif Razavian, H. Azizpour, J. Sullivan, and S. Carlsson. Cnn features off-the-shelf: an astounding baseline for recognition. In *Proceedings of the IEEE conference on computer vision and pattern recognition workshops*, pages 806–813, 2014. 6
- [28] K. Simonyan and A. Zisserman. Very deep convolutional networks for large-scale image recognition. *arXiv preprint arXiv:1409.1556*, 2014. 4
- [29] C. Su, S. Zhang, J. Xing, W. Gao, and Q. Tian. Deep attributes driven multi-camera person re-identification. In *European conference on computer vision*, pages 475–491. Springer, 2016. 3
- [30] C. Szegedy, W. Liu, Y. Jia, P. Sermanet, S. Reed, D. Anguelov, D. Erhan, V. Vanhoucke, and A. Rabinovich. Going deeper with convolutions. In *Proceedings of the IEEE conference on computer vision and pattern recognition*, pages 1–9, 2015. 1
- [31] C. Szegedy, V. Vanhoucke, S. Ioffe, J. Shlens, and Z. Wojna. Rethinking the inception architecture for computer vision. In *Proceedings of the IEEE conference on computer vision and pattern recognition*, pages 2818–2826, 2016. 4, 5
- [32] A. Taha, M. Meshry, X. Yang, Y.-T. Chen, and L. Davis. Two stream self-supervised learning for action recognition. *Deep-Vision Computer Vision and Pattern Recognition Workshop*, 2018. 5

- [33] G. Van Horn, S. Branson, R. Farrell, S. Haber, J. Barry, P. Ipeirotis, P. Perona, and S. Belongie. Building a bird recognition app and large scale dataset with citizen scientists: The fine print in fine-grained dataset collection. In *Proceedings of the IEEE Conference on Computer Vision and Pattern Recognition*, pages 595–604, 2015. [4](#)
- [34] Y. Wang, J. Choi, V. Morariu, and L. S. Davis. Mining discriminative triplets of patches for fine-grained classification. In *Proceedings of the IEEE Conference on Computer Vision and Pattern Recognition*, pages 1163–1172, 2016. [6](#)
- [35] Y. Wen, K. Zhang, Z. Li, and Y. Qiao. A discriminative feature learning approach for deep face recognition. In *European Conference on Computer Vision*, pages 499–515. Springer, 2016. [1](#), [2](#)
- [36] Y. Zhang, X.-S. Wei, J. Wu, J. Cai, J. Lu, V.-A. Nguyen, and M. N. Do. Weakly supervised fine-grained categorization with part-based image representation. *IEEE Transactions on Image Processing*, 25(4):1713–1725, 2016. [6](#)